Reduced Dendritic Spines in the Visual Cortex Contralateral to the Optic Nerve Crush Eye in Adult Mice

Zongyi Zhan,[1] Yali Wu,[1] Zitian Liu,[1] Yadan Quan,[1] Deling Li,[1] Yiru Huang,[1] Shana Yang,[2] Kaili Wu,[1] Lianyan Huang,[3] and Minbin Yu[1]

[1]State Key Laboratory of Ophthalmology, Zhongshan Ophthalmic Center, Sun Yat-sen University, Guangzhou, Guangdong, China
[2]Department of Physiology, Zhongshan School of Medicine, Sun Yat-sen University, Guangzhou, Guangdong, China
[3]Department of Pathophysiology, Zhongshan School of Medicine, Sun Yat-sen University, Guangzhou, Guangdong, China

Correspondence: Minbin Yu, Zhongshan Ophthalmic Center, Sun Yat-sen University, 7 Jinsui Road, Tianhe District, Guangzhou, Guangdong, 510060 China; yuminbin@mail.sysu.edu.cn. Lianyan Huang, Zhongshan School of Medicine, Sun Yat-sen University, 74 Zhongshan Er Road, Yuexiu District, Guangzhou, Guangdong, 510080, China; huangly55@mail.sysu.edu.cn.

Received: April 3, 2020
Accepted: July 31, 2020
Published: August 31, 2020

Citation: Zhan Z, Wu Y, Liu Z, et al. Reduced dendritic spines in the visual cortex contralateral to the optic nerve crush eye in adult mice. *Invest Ophthalmol Vis Sci.* 2020;61(10):55. https://doi.org/10.1167/iovs.61.10.55

Purpose. To determine alteration of dendritic spines and associated changes in the primary visual cortex (V1 region) related to unilateral optic nerve crush (ONC) in adult mice.

Methods. Adult unilateral ONC mice were established. Retinal nerve fiber layer (RNFL) thickness was measured by spectral-domain optical coherence tomography. Visual function was estimated by flash visual evoked potentials (FVEPs). Dendritic spines were observed in the V1 region contralateral to the ONC eye by two-photon imaging in vivo. The neurons, reactive astrocytes, oligodendrocytes, and activated microglia were assessed by NeuN, glial fibrillary acidic protein, CNPase, and CD68 in immunohistochemistry, respectively. Tropomyosin receptor kinase B (TrkB) and the markers in TrkB trafficking were estimated using western blotting and co-immunoprecipitation. Transmission electron microscopy and western blotting were used to evaluate autophagy.

Results. The amplitude and latency of FVEPs were decreased and delayed at 3 days, 1 week, 2 weeks, and 4 weeks after ONC, and RNFL thickness was decreased at 2 and 4 weeks after ONC. Dendritic spines were reduced in the V1 region contralateral to the ONC eye at 2, 3, and 4 weeks after ONC, with an unchanged number of neurons. Reactive astrocyte staining was increased at 2 and 4 weeks after ONC, but oligodendrocyte and activated microglia staining remained unchanged. TrkB was reduced with changes in the major trafficking proteins, and enhanced autophagy was observed in the V1 region contralateral to the ONC eye.

Conclusions. Dendritic spines were reduced in the V1 region contralateral to the ONC eye in adult mice. Reactive astrocytes and decreased TrkB may be associated with the reduced dendritic spines.

Keywords: optic nerve crush, primary visual cortex, dendritic spines

Unraveling the experience-dependent synaptic plasticity of the visual cortex is important for understanding both healthy and abnormal vision. Although experience-dependent synaptic plasticity predominantly occurs early in critical periods, it is considered to be alterable in the adult visual cortex.[1] Monocular deprivation (MD) is used widely for studying experience-dependent synaptic plasticity in the visual cortex,[2,3] but MD after the critical period in rodents tends to be partially reversible later.[4–6] Therefore, MD is not an ideal model for studying changes in plasticity in the primary visual cortex (V1 region) due to permanent visual loss resulting from optic neuropathies, optic nerve trauma, and glaucoma. Optic nerve crush (ONC) in rodents is widely used as a model to investigate the neurodegeneration in the central nervous system (CNS) due to irreversible axonal injury. It is well established that optic nerve injury in adults is associated with an alteration in the V1 region in the CNS.[7–10] However, few studies have investigated the changes of changes in spine density in the V1 region after ONC.

The formation and elimination of dendritic spines are key aspects of synaptic plasticity.[11,12] Dendritic spines in neurons interact with nearby cells such as astrocytes, oligodendrocytes, and microglia in the microenvironment via complex mechanisms.[13–15] Multiple studies have reported important dual roles of astrocytes in dendritic spine modulation in vitro and in vivo.[13,16–18] A1 reactive astrocytes in ischemic central nervous system diseases are induced by activated microglia, which are thought to promote the elimination of dendritic spines and the death of neurons and oligodendrocytes,[17,19] whereas A2 reactive astrocytes are thought to be protective.[20] The activated microglia can change their motility and phagocytic activity to eliminate dendritic spines when responding to varying light and visual stimulation.[15] The role of oligodendrocytes in the formation and elimination of dendritic spines is not clear, but their membrane

Copyright 2020 The Authors

This work is licensed under a Creative Commons Attribution-NonCommercial-NoDerivatives 4.0 International License.

Downloaded from iovs.arvojournals.org on 01/17/2022

proteins, such as Nogo-A, can suppress the formation of dendritic spines.[14] Moreover, astrocytes contain and recycle the nearby precursor form of brain-derived neurotrophic factor (pro-BDNF) to regulate the amount of BDNF.[21] BDNF is a key factor in regulating the maturation of dendritic spines through tropomyosin receptor kinase B (TrkB) in BDNF/TrkB signaling, which has a direct effect on dendritic spines involved in both endocytosis and autophagy.[11,22] Activated TrkB is subsequently endocytosed or ubiquitinated, allowing for either retrograde transport on endosomes to maintain dendritic spine growth or transport in endosomes to lysosomes to eliminate the dendritic spines.[23–25] Although autophagy is known to have a bidirectional effect on synaptic plasticity, decreased autophagy has been proven to be essential for BDNF/TrkB-induced dendritic spine formation.[26]

Accordingly, in vivo two-photon imaging was used to determine changes in dendritic spines in the V1 region contralateral to the ONC eye in adult mice. Alteration of neurons, reactive astrocytes, activated microglia, and oligodendrocytes in the bilateral V1 region were observed, and changes in TrkB, endocytosis, and autophagy in the V1 region contralateral to the ONC eye were investigated.

Methods

Animals and Anesthesia

Four-month-old wild-type C57BL/6 mice of both sexes were purchased from the Guangdong Medical Laboratory Animal Center in China and were examined via flash visual evoked potentials (FVEPs), spectral-domain optical coherence tomography (SD-OCT), immunohistochemistry (IHC), immunofluorescence staining, western blotting, transmission electron microscopy, and coimmunoprecipitation (co-IP). Both sexes of Thy1-YFP transgenic mice (YFP-H-Line), in which the pyramidal cells express yellow fluorescent protein, were obtained from L.Y. Huang at the Zhongshan School of Medicine, Sun Yat-sen University, and were used for two-photon microscopy (TPM) imaging. The Thy1-YFP transgenic mice were genetically edited based on the C57BL/6 mouse background and were backcrossed with C57BL/6J mice for three or four generations. The total number of mice used was 110, including 95 C57BL/6 mice and 15 Thy1-YFP transgenic mice. The FVEPs and SD-OCT examinations utilized five C57BL/6 mice; paraffin IHC, 25 C57BL/6 mice; fluorescence IHC, 25 C57BL/6 mice; western blotting and co-IP, 25 C57BL/6 mice; transmission electron microscopy, 15 C57BL/6 mice; and two-photon imaging, 15 Thy1-YFP transgenic mice. Among these Thy1-YFP transgenic mice, three mice were excluded because of a neovascular membrane covering the cranial window, three mice were excluded because of tissue edema in the V1 region, and one mouse died during the two-photon imaging.

The anesthesia used for TPM imaging was intraperitoneal injection of Avertin. Avertin is not recommended for repeated anesthesia unless necessary because of the risks of peritonitis, ileus, intestinal adhesion, and even death. The use of Avertin was reported to the Animal Ethics Committee of Zhongshan Ophthalmic Center, Sun Yat-sen University. The preparation, storage, and use of Avertin were conducted under close supervision, and, after the Avertin injections, the animals were closely monitored. In our study, no animal died because of the use of Avertin. All of the experiments were approved by Zhongshan Ophthalmic Center, Sun Yat-sen University, and performed in accordance with the ARVO Statement for the Use of Animals in Ophthalmic and Vision Research.

Optic Nerve Crush Surgery

Wild-type C57BL/6 mice and Thy1-YFP transgenic mice were intraperitoneally injected with Avertin (250 mg/kg). As previously described,[27–29] after the mice were anesthetized, the lower bulbar conjunctiva of the mice was incised by 180°, and the optic nerve of the left eye was carefully exposed, avoiding the bleeding. Next, the optic nerve was crushed with cross-action forceps 1 to 2 mm behind the eyeball for 5 seconds. Tobramycin and dexamethasone ointment were applied to both eyes to prevent cornea drying and infection.

In Vivo Long-Term Transcranial Two-Photon Imaging

Based on previous studies,[3,30–32] a modified surgery was applied (Supplementary Fig. S1). Thy1-YFP transgenic mice were deeply anesthetized with an intraperitoneal injection of Avertin (250 mg/kg) and were administered a one-third dose every 30 minutes. The hair on the mouse's head was shaved, and the periosteum was exposed with a midline scalp incision of the skin. The periosteum tissue over the skull surface was removed by toothed forceps. The right-side V1 region was identified based on stereotactic coordinates (2.7 mm lateral to midline and 3.5 mm posterior to the bregma) and was marked. A head holder containing a metal ring with two bars, which weighed 1.2 g, was attached to the mouse's skull with glue (Loctite 495, Henkel, Dusseldorf, Germany), and the center of the head holder was placed on the marked area to restrain the head. When the glue had dried, a dental drill was applied to thin the marked skull, and the round skull area was then peeled off with microforceps. The dura over the exposed cortex was partially removed to avoid bleeding and the formation of neovascular membrane while also allowing the observation area to be more clearly visualized. A glass coverslip of a size larger than the exposed cortex was placed on the exposed cortex and sealed with glue. Next, the mouse was administered a subcutaneous injection comprised of Tolfedine (4 mg/kg), Butomidor (2 mg/kg), and Baytril (5 mg/kg) every 3 days to prevent inflammation, pain, and infection.

Image stacks of the dendritic segments located in the superficial cortical layer were obtained using TPM (FVMPE-RS multiphoton laser scanning microscope; Olympus, Tokyo, Japan) with the laser tuned to 920 nm (25× objective and numerical aperture of 1.05) immersed in artificial cerebrospinal fluid. A 1× digital zoom was used to yield images suitable for quantification of dendritic spines (509.117 µm × 509.117 µm; 2048 × 2048 pixels; 0.75-µm Z step size). The above procedure was repeated, and localization of the same region was performed in the same mice after the first imaging at 1 week and at 2, 3, and 4 weeks. The images were analyzed using Image J software (National Institutes of Health, Bethesda, MD, USA). Filopodia were identified as long, thin protrusions and the remaining protrusions were identified as spines.[3,27,30] Spines were considered different if they were more than 0.7 µm away from their expected positions based on the previous viewing. More than 60 dendritic spines were analyzed from each

Investigative Ophthalmology & Visual Science

Downloaded from iovs.arvojournals.org on 01/17/2022

mouse. The minimum length of dendritic branches included in the analysis was more than 30 µm. The degree of spine formation or elimination was calculated as the number of spines added or eliminated divided by the total number of pre-existing spines.[27,28] Image J software was used to process the image and calculate the dendrite spines.

FVEP Examination

FVEPs were examined using a RETI-port/scan 21 (Roland Consult Stasche & Finger GmbH, Brandenburg, Germany) in accordance with the standards of the International Society for the Clinical Electrophysiology of Vision at specific time points (0 day, 1 week, 2 weeks, 3 weeks, and 4 weeks) as a previous study described.[33] The C57BL/6 mice were dark adapted overnight and then anesthetized with pentobarbital sodium (80 mg/kg) intraperitoneally. Three silver electrodes were implanted supraperiosteally at each hemisphere V1 region, the midpoint of the binoculars, and the tail of the mice. The machine automatically corrected amplitude fluctuations, and an alarm sounded if the electrodes were placed incorrectly. The right eye was patched with a homemade eye mask while the left eye was examined. The eye mask was lightproof and was made with tinfoil, wax, and medical tape. The body temperature of the mouse was maintained at 37°C during the experiments. The test room was illuminated with a dim red light. White flash stimuli were shown at a frequency of 2 Hz for 250 ms. The responses were amplified 10,000 times and bandpass-filtered from 1 to 1000 Hz, and the superposition was conducted 100 times. The parameters recorded were N1 latency, P1 latency, and N1–P1 amplitude (from the N1 wave peak to the P1 wave trough). All of the parameter values were automatically measured by computer output, and the average of the three successive measurements at different consecutive time points of each mouse was calculated.

Retinal Nerve Fiber Layer Thickness Measurement

SD-OCT (Spectralis OCT; Heidelberg Engineering, Heidelberg, Germany) was applied to measure changes in the retina nerve fiber layer (RNFL) thickness of the optic nerve head (ONH) as the pervious study described.[29] After intraperitoneal injection with pentobarbital sodium (80 mg/kg), the mice pupils were dilated using a topical eyedrop of tropicamide phenylephrine. A carboxymethylcellulose sodium eyedrop was used to avoid dryness of the cornea. The mice were placed on a stage that allowed for free rotation to acquire images centered on the ONH. Thickness data were automatically obtained by the software, and the measurements at different consecutive time points for each mouse were recorded.

Tissue Preparation

The C57BL/6 mice were anesthetized with intraperitoneal injections of pentobarbital sodium and were transcardially perfused with normal saline followed by 4% paraformaldehyde (PFA). The brains were carefully removed and immersed in the 4% PFA overnight, and then they were dehydrated and embedded in paraffin or Tissue-Tek OCT compound. For paraffin IHC, 5-µm coronal sections were prepared; for fluorescence IHC, 20-µm coronal frozen sections were prepared. For transmission electron microscopy, the animal was transcardially perfused with PBS followed by 2% PFA and 2.5% glutaraldehyde under anesthesia. The 1-mm^3 visual cortex of the V1 region was quickly removed and immersed in the 2.5% glutaraldehyde. The brains samples were prepared at each time point for different groups of mice (normal control, ONC at 3 days, ONC at 1 week, ONC at 2 weeks, and ONC at 4 weeks).

Immunohistochemistry

For paraffin IHC, the sections were sequentially deparaffinized and hydrated, and antigen was retrieved with 10-mM sodium citrate. The sections were then incubated in 3% hydrogen peroxide for 10 minutes and washed twice using distilled water. Each section was blocked with animal-free blocking solution (15019; Cell Signaling Technology, Boston, MA, USA) for 1 hour at room temperature (RT) and then incubated with primary antibody NeuN (A0951, 1:300; ABclonal, Wuhan, Hubei, China), glial fibrillary acidic protein (GFAP, 12389, 1:200; Cell Signaling Technology), and CNPase (5664, 1:100; Cell Signaling Technology) overnight at 4°C. After three rinses in Tris-buffered saline (TBS), SignalStain Boost IHC Detection Reagent (8114; Cell Signaling Technology) was applied at RT for 30 minutes. After three washes, 3,3′-diaminobenzidine (DAB, G1212-200; Servicebio, Wuhan, Hubei, China) was added until an acceptable staining intensity was reached. The sections were counterstained in hematoxylin. The sections were covered with coverslips using SignalStain mounting medium (14177; Cell Signaling Technology). For fluorescence IHC, the frozen sections were blocked with 10% normal goat serum for 1 hour at RT and then incubated with primary antibody CD68 (ab53444, 2.5 µg/mL; Abcam, Cambridge, UK) overnight at 4°C. After three washes with PBS, Goat anti-Rat IgG Secondary Antibody, Alexa Fluor 488 (bs-0293G-AF488, 1:500; Bioss Antibodies, Beijing, China) was applied. The tissues were incubated at RT in the dark for 2 hours, and the coverslip slides were applied with antifade reagent with 4′,6-diamidino-2-phenylindole (DAPI, 8961; Cell Signaling Technology).

To examine different cells in the visual cortex of both sides, we first compared the IHC staining section with *Paxinos and Franklin's the Mouse Brain in Stereotaxic Coordinates*, 4th Edition[34], and the *Allen Mouse Brain Coronal Atlas* (https://mouse.brain-map.org/static/atlas) to ensure that the area under observation was located at the V1 region. The sections from each animal were studied at intervals of 30 µm, and the sections from different animals were studied at intervals of 100 µm. The stereotaxic coordinates of each IHC staining section were recorded, and sections from different animals with the same stereotaxic coordinates were grouped together for the experiments. We then selected the V1 regions circumscribed with a rectangle outlined with a red-dashed line to analyze the changes in the neuronal cells. The area we examined included cells in layers 2 to 6. To better illustrate the layers and regions, we used a paraffin section with Nissl staining (Fig. 1). In the figures presented in this article, we chose to enlarge identical areas to show the details more clearly. The NeuN staining counts and staining area calculations were processed by Image J software. The staining areas of GFAP, CNPase, and CD68 were qualified by using Image J software and an IHC toolbox plug-in. The areas were expressed as a percentage of the total evaluated area.

We analyzed 101 sections. Among these 101 sections, one section from one animal was used for Nissl staining (Fig. 1);

Investigative Ophthalmology & Visual Science

Downloaded from iovs.arvojournals.org on 01/17/2022

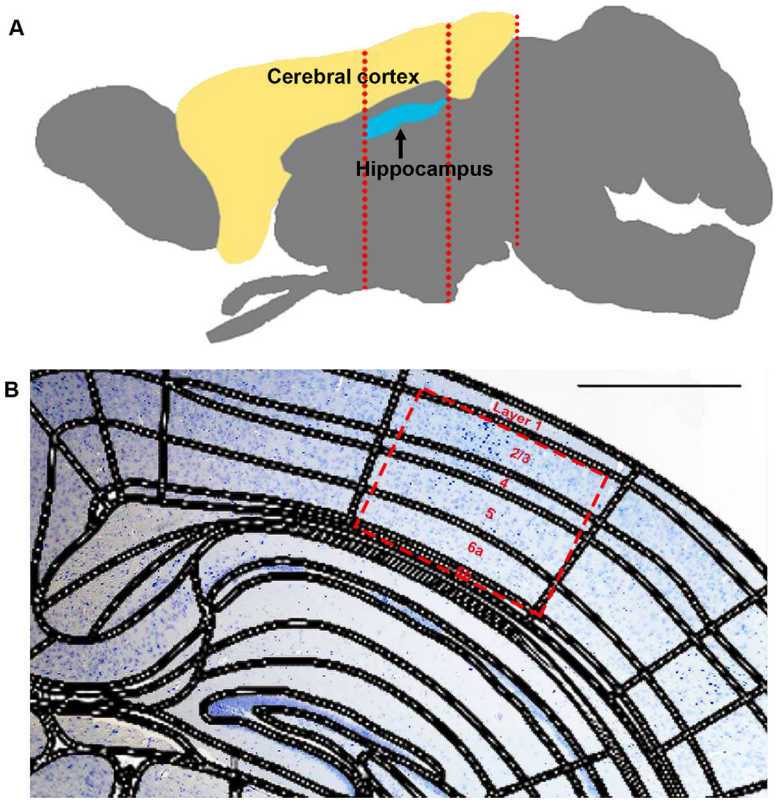

Figure 1. Illustration of regions that were selected for neuronal cell examinations. (**A**) The brain tissues between the *red-dashed lines* were divided into histologic sections according to the stereo-position of the V1 region, which began above the hippocampus and terminated at the end of the occipital lobe. (**B**) This Nissl staining section was first matched with information in *Paxinos and Franklin's the Mouse Brain in Stereotaxic Coordinates*, 4th Edition (bregma, –2.53 mm; interaural, 1.26 mm). The neuronal cells at layer 2-6b in the V1 region (*red-dashed-line rectangle*) were then examined. *Scale bar*: 500 µm.

25 sections from 25 animals were used for NeuN staining (see Fig. 3); 25 sections from the same 25 animals were used for GFAP staining (see Fig. 5); 25 sections from the same 25 animals were used for CNPase staining (see Fig. 6); and 25 sections from another 15 animals were used for CD68 staining (see Fig. 7).

Coimmunoprecipitation and Western Blotting

Protein lysates of the contralateral (right side) V1 region were extracted from tissues by incubating in lysis buffer for western blotting and IP (P0013; Beyotime, Shanghai, China) supplemented with phenylmethylsulfonyl fluoride (ST506; Beyotime) as in previously established procedures.[33] For co-IP, a total amount of 500 µg protein lysate was combined with 5 µg antibody and then diluted with IP lysis/wash buffer to 500 µL. The mixtures were incubated for 2 hours at RT. Protein A/G Magnetic Beads (Pierce Classic Magnetic IP/Co-IP Kit, 88804; Thermo Fisher Scientific, Waltham, MA, USA) were used to absorb the bound protein for 1 hour at RT. The bound proteins were then eluted by low-pH elution. A magnetic stand was used to collect the beads. The eluted proteins were separated using sodium dodecyl sulfate–polyacrylamide gel electrophoresis (SDS-PAGE) and analyzed by western blotting. The following antibodies were used: Rab7 (ab50533, 10 µg/mL; Abcam), Rab11 (5589, 1:50; Cell Signaling Technology), TrkB (ab18987, 2 µg/mL; Abcam), IgG (ab172730, 10 µg/mL; Abcam), and VeriBlot (ab131366, 1:4000; Abcam).

Briefly, equal amounts of proteins were separated in 10% or 12% SDS-PAGE gels and transferred to an Immobilon-PSQ 0.2-µm pore size polyvinylidene fluoride (PVDF) membrane (ISEQ00005; Millipore, Burlington, MA, USA) or an Immobilon-P 0.45-µm pore size PVDF membrane (IPVH00010; Millipore) using Trans-Blot SD Semi-Dry Electrophoretic Transfer Cell (Bio-Rad, Hercules, CA, USA). The membranes were blocked using 5% BSA or 5% fresh skim milk for 2 hours at RT and incubated with selected primary antibodies for 1 hour at RT and then at 4°C overnight. The membranes were washed in TBS with 0.1% Tween-20 and incubated with secondary antibodies for 1 hour at RT. Finally, the membranes were washed and imaged using the Bio-Rad ChemiDoc Touch Imaging System. The protein levels were quantified by densitometry and normalized to glyceraldehyde-3-phosphate dehydrogenase (GAPDH) or β-actin. The light chain 3 (LC3)-II levels were normalized to total LC3 levels. Primary antibodies against the following were used: Beclin 1 (3738, 1:800; Cell Signaling Technology); LC3A/B (12741, 1:800; Cell Signaling Technology); Ndfip1 (DF4681, 1:600; Affinity Biosciences, Cincinnati, OH, USA); Rab5 (AF4073, 1:800; Affinity Biosciences); Rab7 (ab50533, 0.5 µg/mL; Abcam); Rab11 (3539, 1:800; Cell Signaling Technology); TrkB (ab18987, 2 µg/mL; Abcam); GAPDH (14C10, 1:1000; Cell Signaling Technology); and β-actin (4967, 1:1000; Cell Signaling Technology). The secondary antibody was HRP-conjugated Goat Anti-Rabbit IgG (H+L) HRP (S0001, 1:5000; Affinity Biosciences). The band density was calculated by Image J software.

Downloaded from iovs.arvojournals.org on 01/17/2022

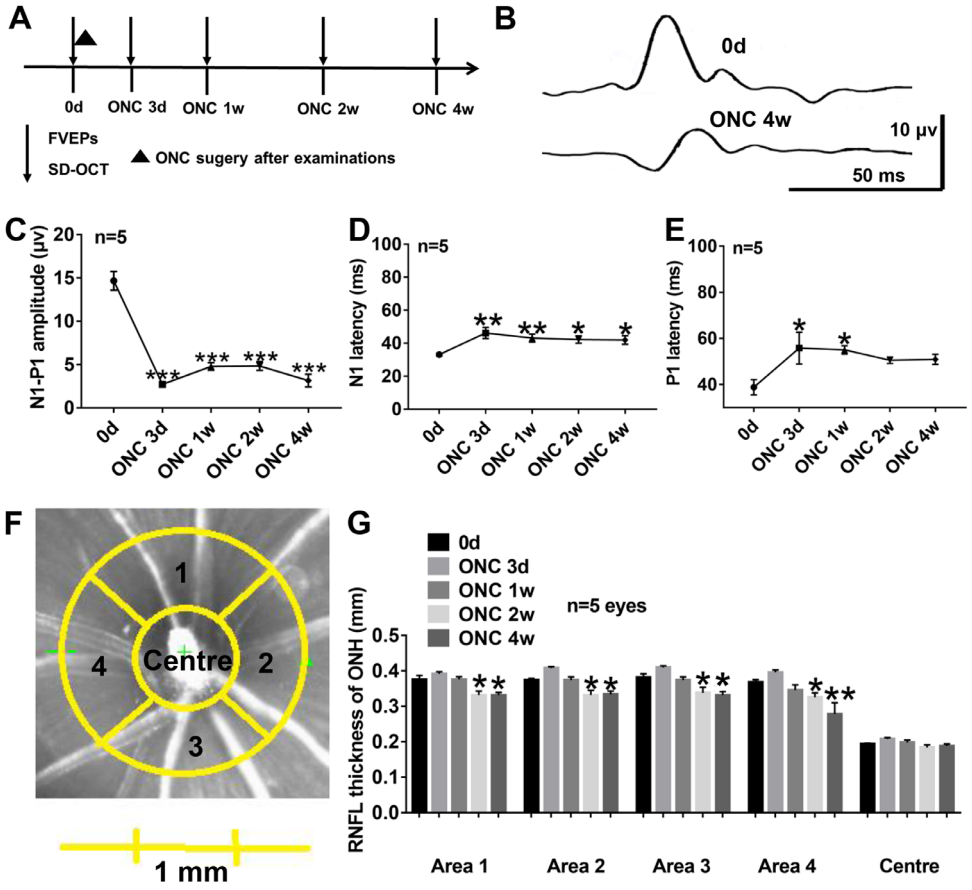

Figure 2. Alterations in FVEPs and RNFL after ONC. (**A**) Experimental timeline over the course of the experiment. FVEPs and SD-OCT were examined on day 0, 3 days after ONC, 1 week after ONC, 2 weeks after ONC, and 4 weeks after ONC. ONC surgery was performed at day 0 immediately after FVEP and SD-OCT examinations. (**B**) Example of FVEPs from a single mouse at day 0 and 4 weeks after ONC. *Scale bar*: 10 μV, 50 ms. (**C**) N1 latency change over 4 weeks following ONC surgery. (**D**) P1 latency change over 4 weeks following ONC surgery. (**E**) N1–P1 amplitude change over 4 weeks following ONC surgery. (**F**) Schematic showing partitions in the SD-OCT examinations. (**G**) RNFL thickness changes in various areas over 4 weeks following ONC surgery. Summary data are presented as mean ± SEM. $^{*}P < 0.05$, $^{**}P < 0.001$ compared with day 0 ($n = 5$ animals per group).

Transmission Electron Microscopy

The 1-mm3 samples from the contralateral (right side) V1 region were sent to Wuhan Servicebio Technology for processing prior to being observed with an HT7700 transmission electron microscope (Hitachi, Tokyo, Japan). The initial autophagic compartments were identified as containing rough endoplasmic reticulum and a mitochondrion.[35,36] The late autophagic compartments contained partially degraded, electron-dense ribosomes.[35,36] To reduce the bias of images readers, a double-blind method was applied. Five random, non-overlapping images were taken of V1 tissues from three animals in each group by a pathologist who was blind to the grouping and experimental design. A total of 75 neurons images were taken to analyze the autophagy. The count of secondary lysosomes, early autophagic compartments, and late autophagic compartments were determined by two readers who were blind to the grouping.

Statistical Analysis

One-way or two-way ANOVA followed by Bonferroni's multiple comparison test was performed (Figs. 2, 3; see also Figs. 5–9). Two-tailed paired *t*-tests were performed (Fig. 4). Data were analyzed using Prism 7.0 (GraphPad, San Diego, CA, USA). All of the data were considered statistically significant at $P < 0.05$.

Results

Abnormal FVEPs and Reduced ONH RNFL Thickness After ONC

Five eyes from five mice were included in 4-week FVEP and SD-OCT examinations (Fig. 2A), and the examinations corresponded to the different time points in the same animal. The representative results of a mouse are shown in Figure 2B. At day 0, the N1, P1, and N1–P1 amplitudes presented as normal, but 4 weeks after ONC, the N1 and P1 latencies were delayed, and the N1–P1 amplitude was reduced. A significant increase in the N1 latency was observed at 3 days, 1 week, 2 weeks, and 4 weeks after ONC, $F(4, 20) = 4.091$, $P = 0.0139$; Bonferroni's multiple comparisons $P = 0.0004$, $P = 0.0051$, $P = 0.0182$, and $P = 0.0234$, respectively (Fig. 2C). Significantly elevated latency was also observed in the P1 latency at 3 days and 1 week after ONC, and the latency did not increase at 2 weeks and 4 weeks after ONC,

Investigative Ophthalmology & Visual Science

Downloaded from iovs.arvojournals.org on 01/17/2022

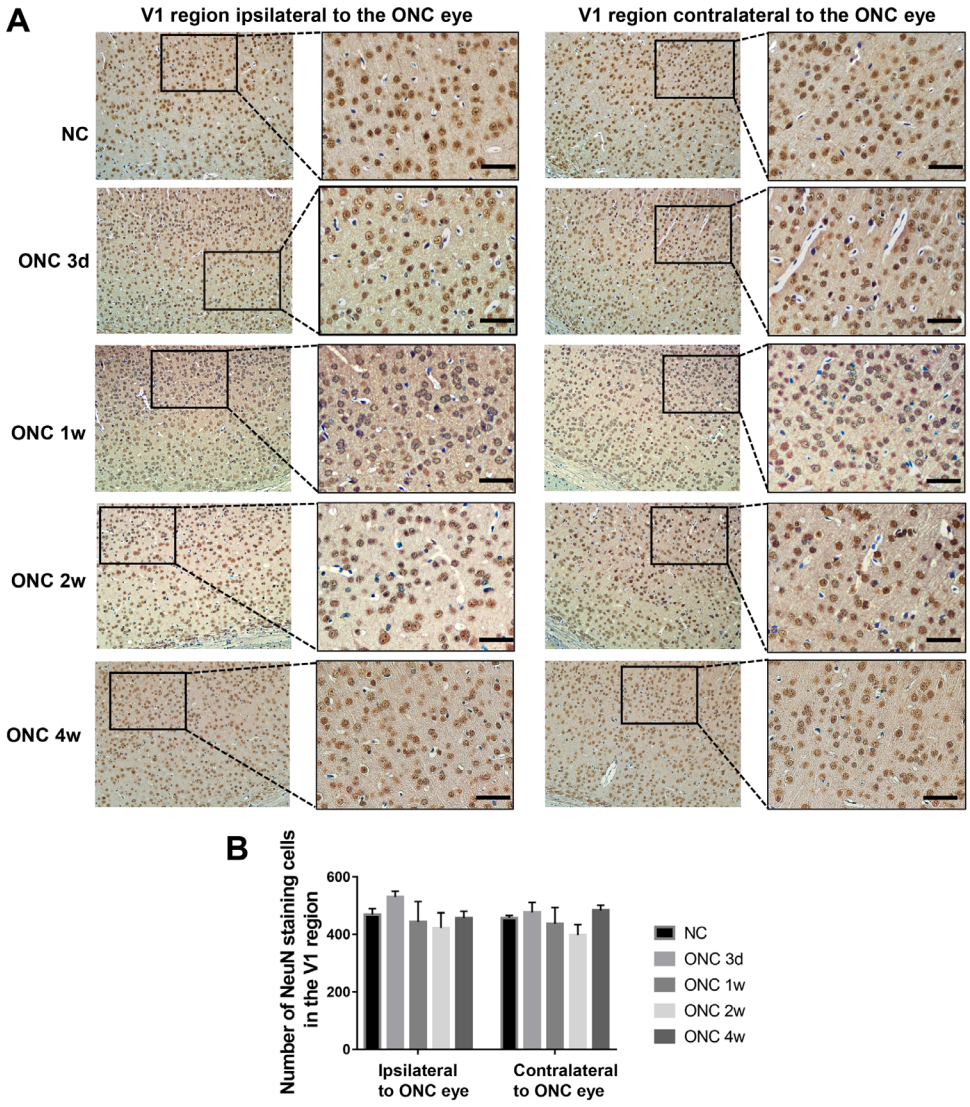

Figure 3. NeuN staining in the bilateral V1 region after unilateral ONC. (**A**) NeuN expression in the NC 3 days after ONC, 1 week after ONC, 2 weeks after ONC, and 4 weeks after ONC at the bilateral V1 region as shown by IHC. (**B**) The counts of NeuN stained cells and densitometric analysis of IHC. *Scale bar*: 50 µm. Summary data are presented as mean ± SEM. $^{*}P < 0.05$, $^{**}P < 0.001$, $^{***}P < 0.0001$ compared with NC group ($n = 5$ animals per group).

$F(4, 20) = 3.708$, $P = 0.0205$; Bonferroni's multiple comparisons $P = 0.0163$, $P = 0.0182$, $P = 0.1270$, and $P = 0.1107$, respectively (Fig. 2D). The amplitude of the N1–P1 wave was also compared at different days after ONC. ONC reduced the amplitude at 3 days, 1 week, 2 weeks, and 4 weeks after ONC, $F(4, 56) = 6.576$, $P = 0.0002$; Bonferroni's multiple comparisons all $P < 0.001$ (Fig. 2E).

The RNFL thickness measurements of the ONH were based on partitions centered on the ONH, which was divided into five zones (Fig. 2F). The longitudinal overall changes of different areas are shown in Figure 2G, $F(4, 20) = 260.5$, $P < 0.001$. There were no changes in the RNFL thickness across areas 1, 2, 3, or 4 at 3 days after ONC (Bonferroni's multiple comparisons $P = 0.6977$, $P = 0.1060$, $P = 0.2298$, and $P = 0.2298$, respectively) and 1 week after ONC (Bonferroni's multiple comparisons $P = 0.9999$, $P = 0.9999$, $P = 0.9619$, and $P = 0.4339$, respectively) compared with those at 0 d. There were significant decreases in RFNL thickness across areas 1, 2, 3, and 4 at 2 weeks after ONC (Bonferroni's multiple comparisons $P = 0.0222$, $P = 0.0312$, $P = 0.0222$, and $P = 0.0312$, respectively) and 4 weeks after ONC (Bonferroni's multiple comparisons $P = 0.0222$, $P = 0.0432$, $P = 0.0075$, and $P < 0.001$, respectively). In addition, the center exhibited no significant change. These results confirmed that the ONC procedures were successful, and obvious decreased RNFL thickness was observed at 2 weeks and 4 weeks after ONC.

Reduced Dendritic Spines in the V1 Region Contralateral to the ONC Eye

To investigate whether ONC affects the total number of neurons in the V1 region, we used the neuron-specific marker NeuN for IHC (Fig. 3A). The results indicate that the number of neurons in the V1 region did not change at different time points after ONC, $F(1, 36) = 0.2991$, $P = 0.5878$; Bonferroni's multiple comparisons all

Investigative Ophthalmology & Visual Science

Downloaded from iovs.arvojournals.org on 01/17/2022

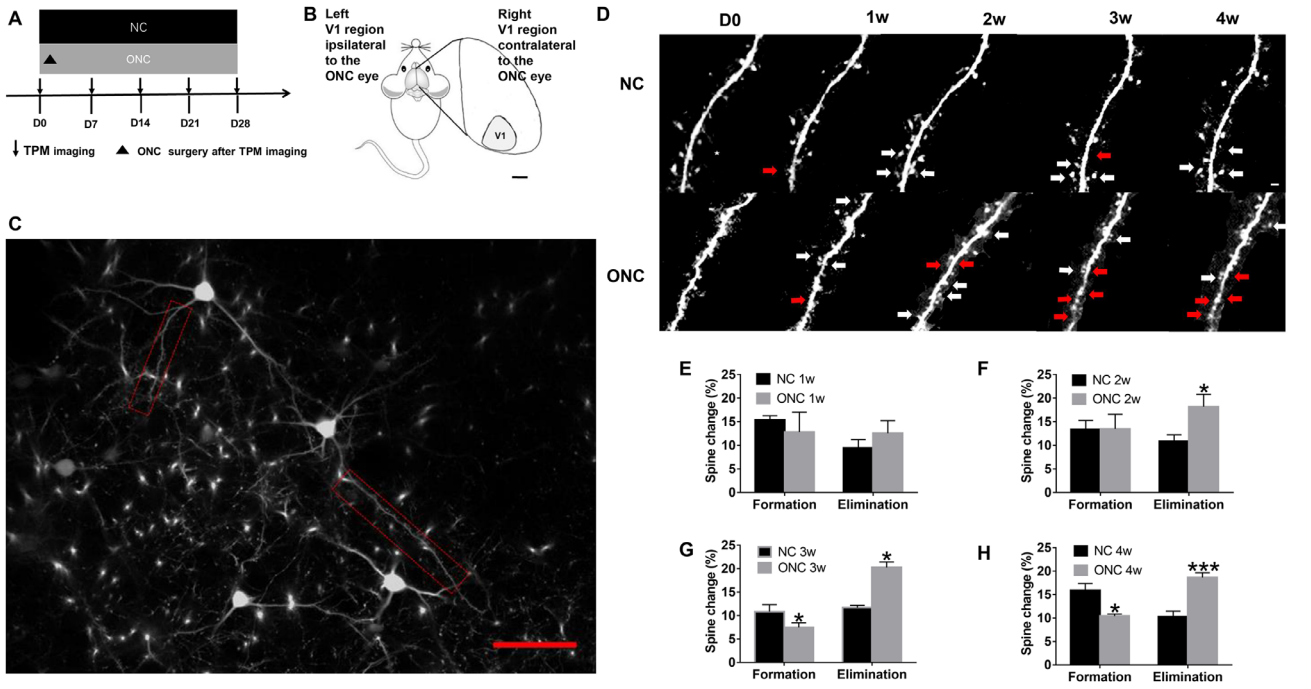

Figure 4. Change in dendritic spines in the V1 region contralateral to the ONC eye. (**A**) Experimental timeline acquired over the course of the experiment. The NC group and ONC group were observed by TPM at day 0, 7, 14, 21, and 28. At day 0, the ONC group received contralateral ONC surgery immediately after two-photon imaging. (**B**) Schematic showing the V1 region contralateral to the ONC eye in the two-photon microcopy examination. *Scale bar*: 1 mm. (**C**) Illustration of spines selected for the data analysis (*red-dashed-line rectangles*). *Scale bar*: 50 µm. (**D**) Images of the dendritic spines in layer 2/3 pyramidal neurons in adult NC and ONC mice over 4 weeks. *Red arrowheads* indicate eliminated dendritic spines, *white arrowheads* indicate newly formed spines, and *white stars* indicate filopodia. *Scale bar*: 2 µm. (**E**) Percentage of dendritic spines eliminated and formed over 1 week in the V1 region contralateral to the ONC eye compared with day 0. (**F**) Percentage of dendritic spines eliminated and formed in the V1 region contralateral to the ONC eye compared with day 7. (**G**) Percentage of dendritic spines eliminated and formed over 3 weeks in the V1 region contralateral to the ONC eye compared with day 14. (**H**) Percentage of dendritic spines eliminated and formed over 2 weeks in the V1 region contralateral to the ONC eye compared with day 28. Summary data are presented as mean ± SEM. $^{*}P < 0.05$, $^{**}P < 0.001$, $^{***}P < 0.0001$ ($n = 4$ animals per groups).

$P > 0.9999$ (Fig. 3B). Hence, we used TPM to visualize the dendritic spines of layer 2 and 3 pyramidal cells in the right side V1 regions over 4 weeks based on the stereotaxic coordinates and the two-photon imaging corresponding to the different time points in the same animal of the non-crush control (NC) group and left-side ONC group (Figs. 4A–4D). The ONC left-side V1 region was identified as the ipsilateral V1 region to the ONC eye, and the right side V1 region was identified as the contralateral V1 region to the ONC eye (Fig. 4B).

In the ONC group, at 1 week there were no significant differences in the spine elimination rate or spine formation rate compared to the NC group (elimination, ONC at 1 week 12.56 ± 1.54% vs. NC at 1 week 9.45 ± 1.01%, $t = 1.265$, $df = 3$, $P = 0.2953$; formation, ONC at 1 week 12.85 ± 2.41% vs. NC at 1 week 15.43 ± 0.49%, $t = 1.097$, $df = 3$, $P = 0.3527$) (Fig. 4E). Two weeks after ONC, a significant increase in the spine elimination rate was observed when compared to that in the NC group. In addition, the spine formation rate was not significantly changed by ONC during the same period (elimination, ONC at 2 weeks 18.21 ± 1.51% vs. NC at 2 weeks 10.83 ± 0.79%, $t = 8.534$, $df = 3$, $P = 0.0034$; formation, ONC at 2 weeks 13.50 ± 1.77% versus NC 2 week 13.43 ± 1.06%, $t = 0.2009$ $df = 3$, $P = 0.8536$) (Fig. 4F). Three weeks after ONC, significant increases in the spine elimination rate and spine formation rate were observed compared to those in the 3-week NC group (elimination, ONC at 3 weeks 20.28 ± 1.16% vs. NC at 3 weeks 11.67 ± 0.52%, $t = 4.986$, $df = 3$, $P = 0.0155$; formation, ONC at 3 weeks 7.47 ± 1.0% vs. NC 3 weeks 10.83 ± 1.50%, $t = 5.977$, $df = 3$, $P = 0.0094$) (Fig. 4G). Furthermore, 4 weeks after ONC, significant alterations were observed in both spine elimination and spine formation rates (elimination, ONC at 4 weeks 18.66 ± 0.58% vs. NC at 2 weeks 10.27 ± 0.68%, $t = 47.85$, $df = 3$, $P < 0.00001$; formation, ONC at 4 weeks 10.43 ± 0.25% vs. NC at 4 weeks 15.90 ± 0.85%, $t = 4.097$, $df = 3$, $P = 0.0263$) (Fig. 4H). These results confirm that in the V1 region contralateral to the ONC eye, 2, 3, and 4 weeks after ONC spine elimination was increased and at 3 and 4 weeks after spine formation was decreased.

Increased Reactive Astrocytes Staining in the V1 Region Contralateral to the ONC Eye

To further investigate whether other cell components in the V1 region changed with the reduction in dendritic spines after ONC, we used specific cell markers (GFAP, CNPase, and CD68) to show the overall staining area of reactive astrocytes, oligodendrocytes, and activated microglia. The staining areas were observed in the bilateral V1 regions.

In the V1 region contralateral to the ONC eye, the staining area of GFAP was significantly increased. In contrast, the staining area did not increase in the V1 region ipsilateral

Investigative Ophthalmology & Visual Science

Downloaded from iovs.arvojournals.org on 01/17/2022

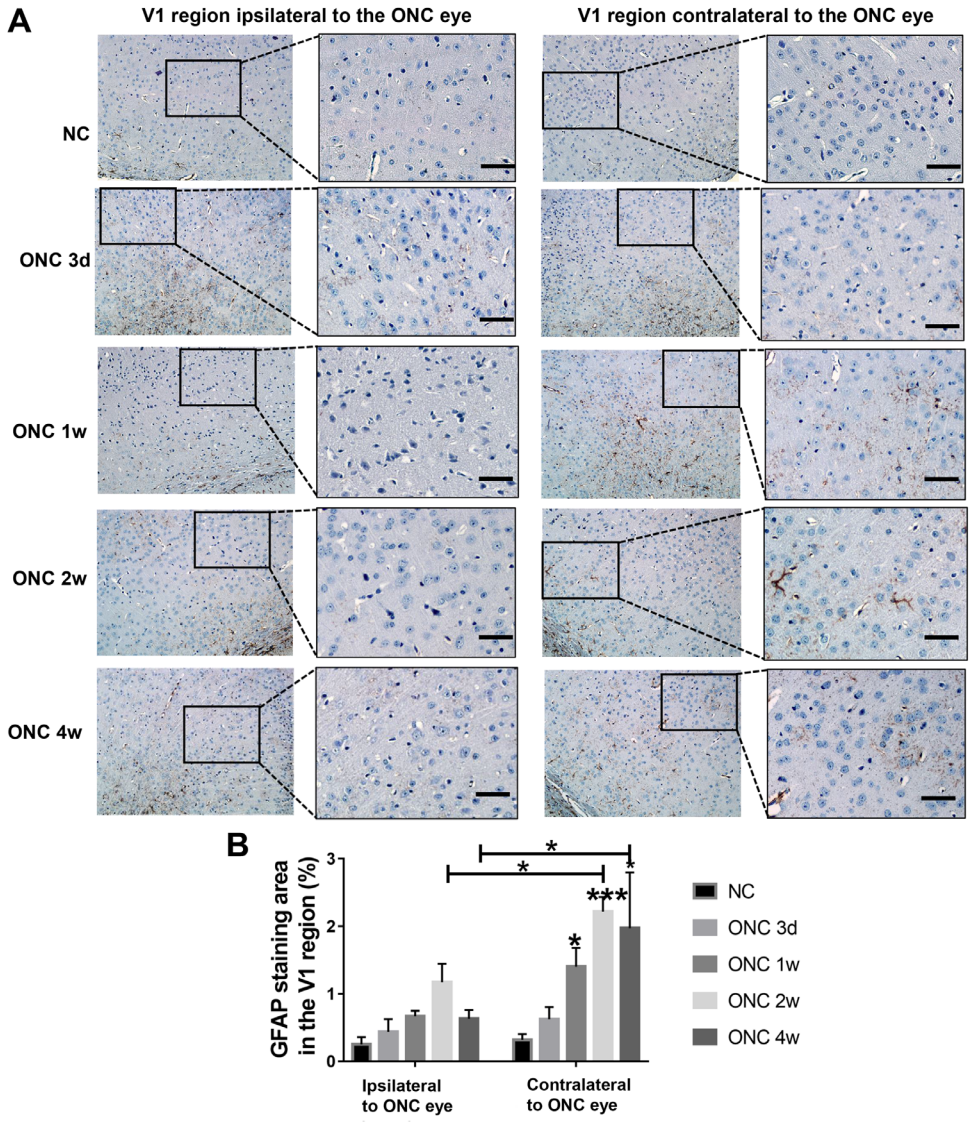

Figure 5. GFAP staining at the bilateral V1 region after unilateral ONC. (**A**) GFAP expression in the NC and groups representing 3 days after ONC, 1 week after ONC, 2 weeks after ONC, and 4 weeks after ONC at the bilateral V1 region as shown by IHC. *Scale bar*: 50 µm. (**B**) GFAP staining area and densitometric analysis of IHC. Summary data are presented as mean ± SEM. $^{*}P < 0.05$, $^{**}P < 0.001$, $^{***}P < 0.0001$ compared with the NC group ($n = 5$ animals per groups).

to the ONC eye, $F(1, 31) = 16.8$, $P = 0.0003$ (Fig. 5), with the following Bonferroni's multiple comparisons: For the V1 region contralateral to the ONC eye, NC versus 3 days after ONC, $P > 0.9999$; NC versus 1 week after ONC, $P = 0.0167$; NC versus 2 weeks after ONC, $P < 0.0001$; and NC versus 4 weeks after ONC, $P = 0.0010$. For the V1 region ipsilateral to the ONC eye, NC versus 3 days after ONC, $P > 0.9999$; NC versus 1 week after ONC, $P = 0.9810$; NC versus 2 weeks after ONC, $P = 0.0735$; and NC versus 4 weeks after ONC, $P > 0.9999$. Additionally, there were significant differences between the contralateral and ipsilateral V1 regions in the GFAP staining area 2 weeks after ONC and 4 weeks after ONC, with the following Bonferroni's multiple comparisons for the V1 region ipsilateral to the ONC eye versus V1 region contralateral to the ONC eye: NC, $P > 0.9999$; 3 days after ONC, $P = 0.9914$; 1 week after ONC, $P = 0.1573$; 2 weeks after ONC, $P = 0.0401$; and 4 weeks after ONC, $P = 0.0103$.

However, no significant differences were seen between the NC and ONC groups at any of the time intervals after ONC in the CNPase staining area, $F(1, 34) = 1.83$, $P = 0.1850$ (Fig. 6), with the following Bonferroni's multiple comparisons: For the V1 region ipsilateral to the ONC eye, all $P > 0.9999$. For the V1 region contralateral to the ONC eye, NC versus 3 days after ONC, $P = 0.7293$; NC versus 1 week after ONC, $P > 0.9999$; NC versus 2 weeks after ONC, $P = 0.5879$; and NC versus 4 weeks after ONC, $P > 0.9999$. For the NC, V1 region ipsilateral to the ONC eye versus V1 region contralateral to the ONC eye, $P = 0.8769$; 3 days after ONC, $P > 0.9999$; 1 week after ONC, $P = 0.9500$; 2 weeks after ONC, $P > 0.9999$; and 4 weeks after ONC, $P > 0.9999$. We estimated the staining area of activated microglia by CD68 staining using fluorescence IHC. As shown in Figure 7, $F(1, 40) = 0.5442$, $P = 0.4650$, no significant difference was observed in

Investigative Ophthalmology & Visual Science

Downloaded from iovs.arvojournals.org on 01/17/2022

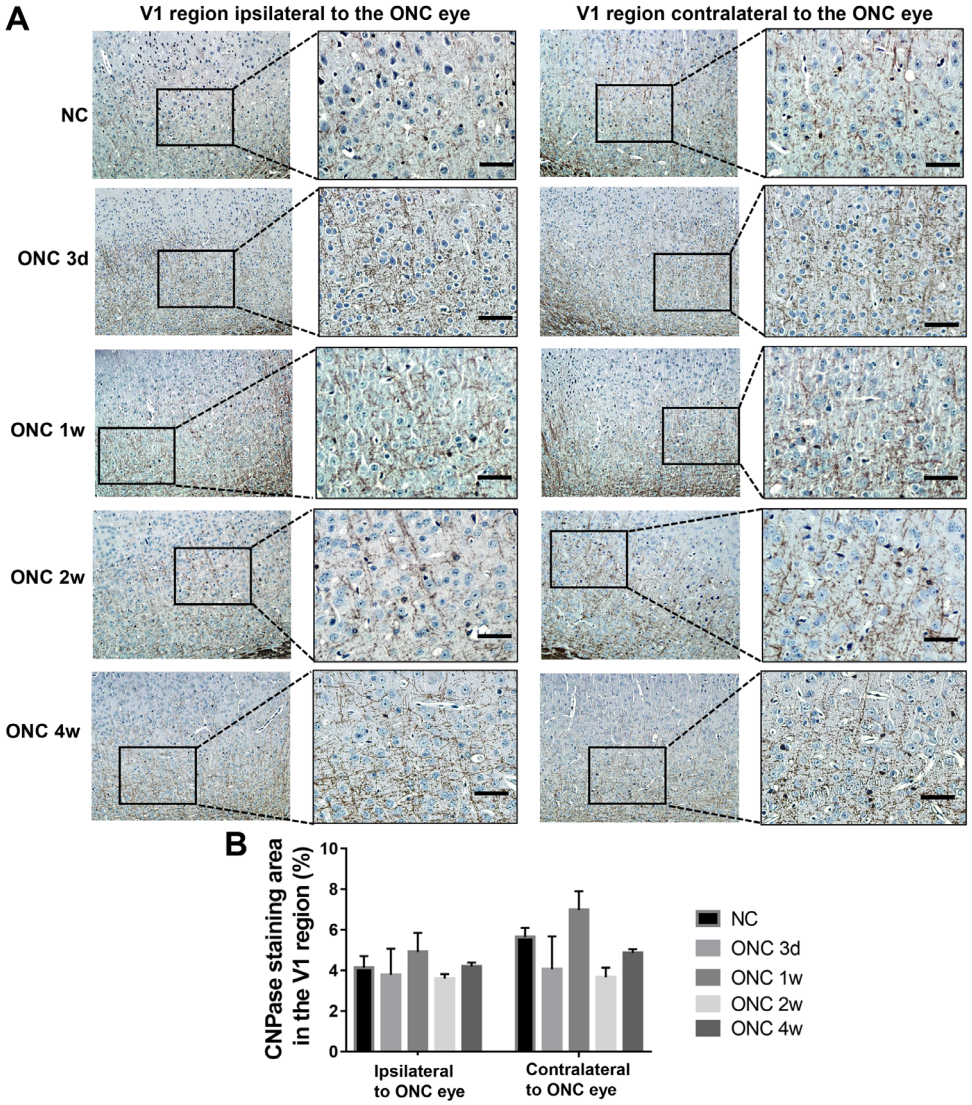

Figure 6. CNPase staining at the bilateral V1 region after unilateral ONC. (**A**) CNPase expression in the NC and groups representing 3 days after ONC, 1 week after ONC, 2 weeks after ONC, and 4 weeks after ONC at the bilateral V1 region as shown by IHC. *Scale bar*: 50 µm. (**B**) CNPase staining area and densitometric analysis of IHC. Summary data are presented as mean ± SEM. $^{*}P < 0.05$, $^{**}P < 0.001$, $^{***}P < 0.0001$ compared with the NC group ($n = 5$ animals per groups).

the CD68 staining area between different groups in the V1 region ipsilateral to the ONC eye versus V1 region contralateral to the ONC eye, with the following Bonferroni's multiple comparisons: For the V1 region ipsilateral to the ONC eye, NC versus 3 days after ONC, $P = 0.5676$; NC versus 1 week after ONC, $P > 0.9999$; NC versus 2 weeks after ONC, $P = 0.9963$; and NC versus 4 weeks after ONC, $P = 0.3449$. For the V1 region contralateral to the ONC eye, NC versus 3 days after ONC, $P > 0.9999$; NC versus 1 week after ONC, $P = 0.9896$; NC versus 2 weeks after ONC, $P = 0.8186$; and NC versus 4 weeks after ONC, $P = 0.7888$. In addition, there was no significant difference between the contralateral and ipsilateral V1 regions in the CD68 staining area, with the following Bonferroni's multiple comparisons: For the V1 region ipsilateral to the ONC eye versus V1 region contralateral to the ONC eye, all $P > 0.9999$, except at 4 weeks after ONC, when $P = 0.2190$. These results suggest that there were reactive astrocytes in the V1 region contralateral to the ONC eye at 2 weeks and 4 weeks after ONC.

Decreased TrkB and Alterations in Major TrkB Trafficking Proteins in the V1 Region Contralateral to the ONC Eye

We estimated the change in TrkB and the related major TrkB trafficking proteins in the endocytic pathway. As shown in Figure 8A, TrkB expression was significantly decreased in the V1 region contralateral to the ONC eye 4 weeks after ONC compared to that in the NC group ($P = 0.0106$) with a total downtrend, $F(4, 10) = 3.921$, $P = 0.0363$. The expression of major proteins in the endocytic pathway (Rab5, Rab7, and Rab11) was also detected. As shown in Figures 8C–8E, the expression of Rab5 did not change significantly ($P = 0.9738$) among the different groups. The expression of Rab7 was significantly elevated, $F(4, 10) = 4.678$, $P = 0.0218$, with the following Bonferroni's multiple comparisons: NC group versus 3 days after ONC, $P = 0.0326$; NC versus 1 week after ONC, $P = 0.0311$; NC versus 2 weeks after ONC, $P = 0.0334$; and NC versus 4 weeks after ONC, $P = 0.0164$. In addition, the expression

Investigative Ophthalmology & Visual Science

Downloaded from iovs.arvojournals.org on 01/17/2022

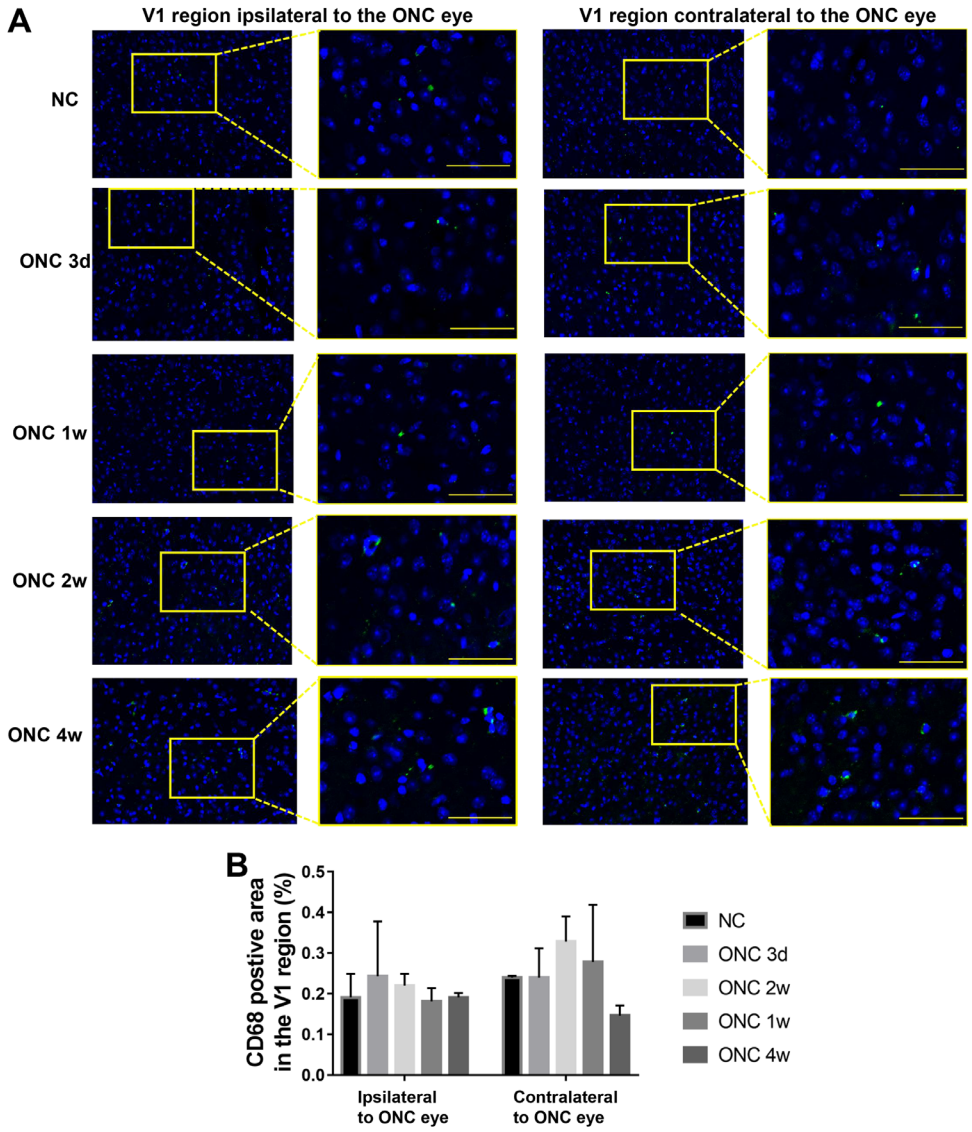

Figure 7. CD68 staining at the bilateral V1 region after unilateral ONC. (**A**) CD68 expression in the NC and groups representing 3 days after ONC, 1 week after ONC, 2 weeks after ONC, and 4 weeks after ONC at the bilateral V1 region as shown by frozen section IHC. *Scale bar*: 50 µm. (**B**) CD68 staining area and densitometric analysis of IHC. Summary data are presented as mean ± SEM. $^{*}P < 0.05$, $^{**}P < 0.001$, $^{***}P < 0.0001$ compared with the NC group ($n = 5$ animals per groups).

of Rab11 was significantly decreased, $F(4, 10) = 9.694$, $P = 0.0018$, with the following Bonferroni's multiple comparisons: NC versus 1 week after ONC, $P = 0.0338$; NC versus 2 weeks after ONC, $P = 0.0031$; and NC versus 4 weeks after ONC, $P = 0.0027$. The elevated Rab7 and decreased Rab11 suggested enhancement of ubiquitinated TrkB targeted to lysosomes; therefore, Ndfip1, a protein that mediates the ubiquitination of TrkB, was assessed (Fig. 8B). The expression levels of Ndfip1 were significantly elevated in the 4 weeks after ONC group compared to the NC group ($P = 0.0329$) with a total uptrend, $F(4, 10) = 3.21$, $P = 0.0613$. Moreover, the co-IP of Rab11 with TrkB was analyzed using both control antibodies and antibodies to TrkB in the NC group and 4 weeks after ONC. As shown in Figure 8F, the interaction of Rab11 and TrkB in the NC group was greater than that in the 4 weeks after ONC group. These results suggest that TrkB was decreased and the related major TrkB trafficking proteins were also correspondingly changed in the V1 region contralateral to the ONC eye after ONC.

Enhanced Autophagy in the V1 Region Contralateral to the ONC Eye

To determine whether autophagy increased, transmission electron microscopy and western blotting were used to examine the samples from the V1 region contralateral to the ONC eye of different groups (NC, 3 days after ONC, 1 week after ONC, 2 weeks after ONC, and 4 weeks after ONC). As shown in Figure 9A, the neurons and organelles appeared normal in the NC group; however, mitochondria displayed swelling and cristae disruption at 1 week, 2 weeks, and 4 weeks after ONC. Quantitative analysis of the changes in the neurons showed that the number of secondary lysosomes, initial autophagic compartments, and late autophagic compartments changed after ONC, $F(2, 134) = 40.26$, $P < 0.001$. The secondary lysosomes appeared more frequently in the post-ONC group and were significantly increased in the 4 weeks post-ONC group compared to those in the NC group ($P = 0.0006$).

Investigative Ophthalmology & Visual Science

Downloaded from iovs.arvojournals.org on 01/17/2022

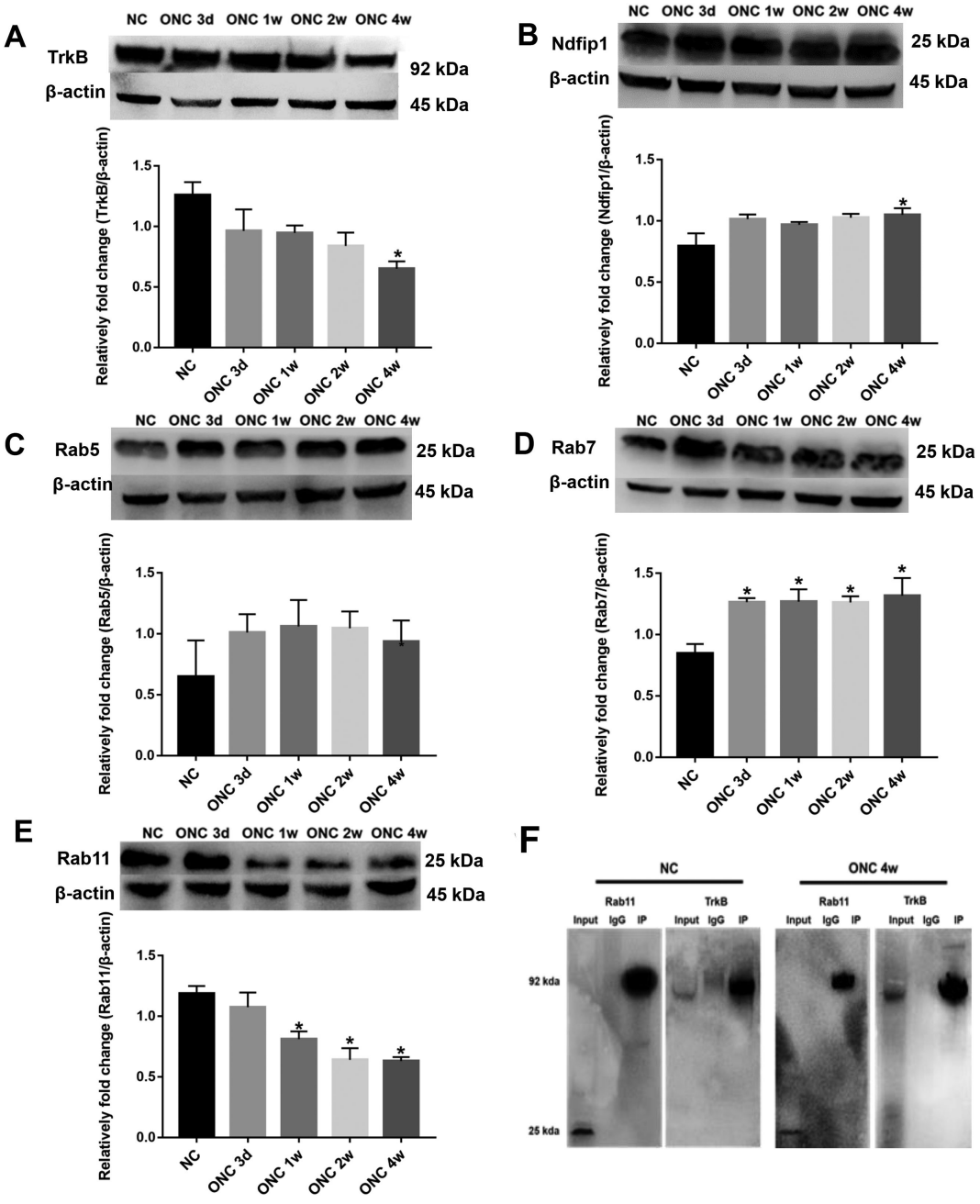

Figure 8. TrkB and related major TrkB trafficking proteins expression in the V1 region contralateral to the ONC eye (**A**–**E**) TrkB, Ndfip1, Rab5, Rab7, and Rab11 expression in the NC and groups representing 3 days after ONC, 1 week after ONC, 2 weeks after ONC, and 4 weeks after ONC in the V1 region contralateral to the ONC eye as shown by western blotting and densitometric analysis of western blotting analysis. (**F**) Interaction between TrkB and Rab11 in the NC and at 4 weeks after ONC in the V1 region contralateral to the ONC eye as shown by co-IP. Summary data are presented as mean ± SEM. $^{*}P < 0.05$, $^{**}P < 0.001$, $^{***}P < 0.0001$ compared with the NC group ($n = 5$ animals per groups).

Moreover, the initial autophagic compartments were increased at 3 days after ONC but did not significantly change at 1 week, 2 weeks, or 4 weeks in the after-ONC groups ($P = 0.9788$, $P = 0.9788$, $P = 0.9788$, and $P = 0.7977$, respectively). The late autophagic compartments increased significantly at 1 week after ONC ($P = 0.0198$) but total LC3 were significantly decreased at 4 weeks after ONC compared to the NC group ($P = 0.0084$) (Figs. 9B, 9D) with a turnover trend, $F(4, 10) = 5.693$, $P = 0.0118$. In addition, the levels of Beclin1 were markedly increased at 4 weeks after ONC compared to the NC group, $F(4, 10) = 13.1$, $P = 0.0005$, Bonferroni's multiple comparisons $P = 0.0004$ (Figs. 9B, 9C). Our results suggest that autophagy was enhanced in the V1 region contralateral to the ONC eye.

Discussion

To the best of our knowledge, this is the first study to demonstrate that long-term vision impairments in

Investigative Ophthalmology & Visual Science

Downloaded from iovs.arvojournals.org on 01/17/2022

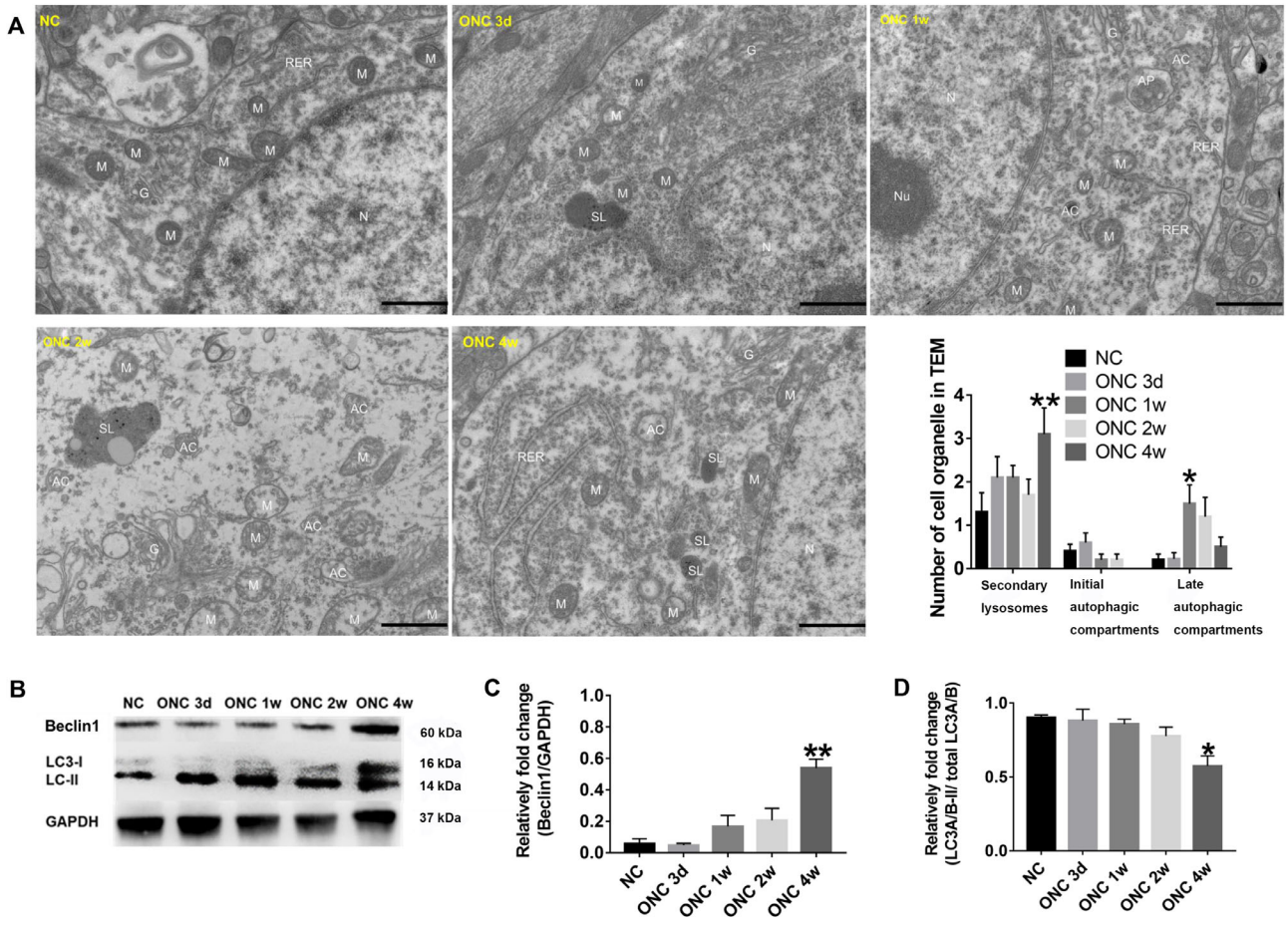

Figure 9. Autophagy in the V1 region contralateral to the ONC eye. (**A**) Representative electron microphotographs of ultrastructural changes in neurons at the V1 region contralateral to the ONC eye and quantitative analysis of the NC and groups representing 3 days after ONC, 1 week after ONC, 2 weeks after ONC, and 4 weeks after ONC. *Scale bar*: 1 µm. N, nucleus; Nu, nucleolus; M, mitochondria; G, Golgi complex; RER, rough endoplasmic reticulum; SL, secondary lysosome; AP, initial autophagic compartment; AC, late autophagic compartments. (**B–D**) Beclin1 and LC3 expression in the NC and groups representing 3 days after ONC, 1 week after ONC, 2 weeks after ONC, and 4 weeks after ONC in the V1 region contralateral to the ONC eye as shown by western blotting and densitometric analysis of the western blotting results. Summary data are presented as mean ± SEM. $^{*}P < 0.05$, $^{**}P < 0.001$, $^{***}P < 0.0001$, compared with the NC group ($n = 5$ animals per groups).

adulthood due to unilateral ONC decrease the dendritic spines in the V1 region contralateral to the ONC eye. The basis of synaptic plasticity is the formation and elimination of dendritic spines.[12] Dendritic spines are variational, exhibiting a transient or persistent lifetime from minutes to years in vivo.[37] Prior studies provided a range of evidence supporting the conclusion that monocular deprivation can induce impairments in dendritic spines in the V1 region of developing animals; however, following binocular recovery in MD juveniles, the size of spines can be recover.[3] Even the reversal of long-term MD by dark exposure and reverse deprivation in adulthood can recover the size and number of spines.[6,38] Moreover, studies of in vivo experience-dependent plasticity have revealed that the dendritic spines of layer 2/3 neurons are plastic during critical periods in rodents, but the dendritic spines of layer 5 are relatively stable in adult rodents.[39,40] On the other hand, spine density and intrinsic spine dynamics were found to be significantly higher in layer 2/3 neurons than in layer 5 neurons in both developing and developed mice.[41] These findings indicate that ONC animals may be a better model to observe the alteration of dendritic spines in layer 2/3 in adulthood when studying optic nerve injury diseases. However, only a few studies have analyzed the alterations of dendritic spines in layer 2/3 in the adult mouse V1 region after ONC.

Having established ONC animals, we used TPM to study the long-term changes in dendritic spines in the V1 region before and after ONC in living adult animals. Similar to MD, ONC induced two separate modifications, including a rapid response and a delayed response. To exclude the rapid response of ONC and simulate optic neuropathy, we observed changes in the spines at 1, 2, 3, and 4 weeks after ONC. This results strongly indicate that dendritic spines were reduced in layer 2/3 of the V1 region contralateral to the ONC eye after ONC. This result is in agreement with a previous study in mice that used MD at postnatal days 9 and 10, and the dendritic spines in layer 2/3 were estimated by DiI labeling for approximately 30 days.[42] Moreover, the results in Figures 2 and 4 suggest that the dendritic spines might be affected by ONC later than the RNFL. Only SD-OCT can show obvious changes in the RNFL.

Additionally, our results demonstrated that reactive astrocyte (GFAP) staining increased in the V1 region contralateral to the ONC eye. It is notable that not all astrocytes express GFAP in the healthy CNS, but during reactive astrogliosis

Investigative Ophthalmology & Visual Science

Downloaded from iovs.arvojournals.org on 01/17/2022

and glial scar formation of neurodegeneration diseases, most astrocytes express GFAP.[43] There are at least two types of reactive astrocytes. A1 reactive astrocytes are more common in ischemic CNS diseases; they contribute to the death of oligodendrocytes and neurons and eliminate dendritic spines, induced by the activated microglia.[17] A2 reactive astrocytes release many neurotrophic factors and regulate brain homeostasis.[44] Moreover, astrocytes make contacts with neurons, which uptake and recycle pro-BDNF after being triggered by stimuli to affect BDNF/TrkB signaling.[21] Previous studies support our results that unilateral ONC can result in injury to the V1 region contralateral to the ONC eye as in other neurodegenerative diseases. Based on this evidence, the increased GFAP staining indicates that the astrocytes may be reactive, affecting BDNF/TrkB signaling and having an impact on dendritic spines.

CNPase, as a structural protein primarily expressed in the myelinating glia, is a specific maker of oligodendrocytes. Oligodendrocytes themselves express growth inhibitors, such as oligodendrocyte–myelin glycoprotein, which has been proven to regulate structural and functional neuronal plasticity both in vitro and in vivo.[14,45] The reason why CNPase remained unchanged in the V1 region may be related to fact that the injury in the ONC model is mechanical and far away from lesions.

Microglia, the resident immune cells of the brain, showed increased phagocytic activity and migration ability in response to injury; they are thought to be able to modify synaptic connections and synaptic dendritic spines.[46] Ninety-four percent of microglial process touch synaptic elements, and the interaction between microglia and neurons has been found to be correlated with both increased growth and elimination of dendritic spines when animals were exposed to visual stimuli.[47] Hence, we used CD68 staining to reveal activated microglia in the V1 region after ONC. The results of our study are in agreement with some previous studies using the MD model.[47–49] The reason why ONC did not activate microglia might be due to the absence of apoptotic neuronal cell death. Another study found that when apoptosis was genetically prevented, microglial activation, in terms of protein expression and proinflammatory cytokine/chemokine production, disappeared.[50] In addition, our findings from NeuN staining also supported this hypothesis.

BDNF/TrkB signaling plays a critical role in the visual pathway. Anterograde BDNF transportation from retina can promote the survival of postsynaptic neurons in the lateral geniculate nucleus (LGN) in developing animals,[51] but depletion of retinal BDNF in developed animals seems to have no effect on the survival of neurons in the LGN.[52] However, intravitreous injection of BDNF prevents the death of LGN neurons after direct trauma in the visual cortex of adult rodents.[53] Ablation of BDNF in the neural lineage also causes an increase in autophagy and a decrease in the number of spines[26]; therefore, it is a matter of some controversy as to whether anterograde BDNF from retina affects the visual cortex directly in developed animals. In developed rodents, ONC induces transient changes in TrkB expression not only in retina but also in superior colliculus. It has been reported that TrkB increased at 6 hours after ONC and decreased at 3 days after ONC.[54] Also, TrkB is reduced in the visual cortex of dark-reared animals compared with light-reared animals.[55] Hence, both depletion of anterograde BDNF from the retina and loss of visual input from the ONC eyes might attribute to the decreased TrkB in our results. It has been found that BDNF/TrkB signaling requires retrograde axonal transport through endosomes and autophagosomes to promote the formation of spines and to counteract neurodegeneration such as Alzheimer's disease and Huntington's disease.[56–58] In brains of Alzheimer's disease patients, the expression of the TrkB protein and gene is reduced with decreased spines density,[59,60] whereas the expression levels of rab5 and rab7 gene are upregulated.[60] Enhanced autophagy in the early stage of Alzheimer's disease can lead to the accumulation of autophagosomes, resulting in damage to neuronal nutrients and organelle circulation, in addition to causing neuronal degeneration.[61] In cells and animal models of Huntington's disease, Rab11 fails to recycle endosomes to the plasma membrane, resulting in reduced cysteine uptake, deficient glutathione synthesis, and repaired synaptic function.[62] Thus, changes in endocytic and autophagic flux may explain the decreased TrkB after ONC in our results (Figs. 8, 9).

Conclusions

This study demonstrated that dendritic spines were reduced in the V1 region contralateral to the ONC eye, which might relate to the reactive astrocytes, decreased TrkB, and changes in endosomes and autophagosomes. Further studies are needed to investigate the specific mechanisms underlying the impairment of dendritic spines after ONC.

Acknowledgments

The authors thank Li Boxing, Qiu Guoguang, Li Juan, Liu Liling, Li Weihua, Yu Huan, Li Zhiquan, and Wu Peixin for their contributions, which enabled some of the work reported here.

Supported by a grant from the National Natural Science Foundation of China (81870655).

Disclosure: **Z. Zhan,** None; **Y. Wu,** None; **Z. Liu,** None; **Y. Quan,** None; **D. Li,** None; **Y. Huang,** None; **S. Yang,** None; **K. Wu,** None; **L. Huang,** None; **M. Yu,** None

References

1. Gilbert CD, Wiesel TN. Receptive field dynamics in adult primary visual cortex. *Nature*. 1992;356:150–152.
2. Hofer SB, Mrsic-Flogel TD, Bonhoeffer T, Hubener M. Lifelong learning: ocular dominance plasticity in mouse visual cortex. *Curr Opin Neurobiol*. 2006;16:451–459.
3. Zhou Y, Lai B, Gan WB. Monocular deprivation induces dendritic spine elimination in the developing mouse visual cortex. *Sci Rep*. 2017;7:4977.
4. Bavelier D, Levi DM, Li RW, Dan Y, Hensch TK. Removing brakes on adult brain plasticity: from molecular to behavioral interventions. *J Neurosci*. 2010;30:14964–14971.
5. Sengpiel F. Plasticity of the visual cortex and treatment of amblyopia. *Curr Biol*. 2014;24:R936–R940.
6. Hosang L, Yusifov R, Lowel S. Long-term visual training increases visual acuity and long-term monocular deprivation promotes ocular dominance plasticity in adult standard cage-raised mice. *eNeuro*. 2018;5:ENEURO.0289–17.2017.
7. Kreutz MR, Seidenbecher CI, Sabel BA. Molecular plasticity of retinal ganglion cells after partial optic nerve injury. *Restor Neurol Neurosci*. 1999;14:127–134.
8. Jaepel J, Hubener M, Bonhoeffer T, Rose T. Lateral geniculate neurons projecting to primary visual cortex show ocular dominance plasticity in adult mice. *Nat Neurosci*. 2017;20:1708–1714.

Downloaded from iovs.arvojournals.org on 01/17/2022

9. Vasalauskaite A, Morgan JE, Sengpiel F. Plasticity in adult mouse visual cortex following optic nerve injury. *Cereb Cortex*. 2019;29:1767–1777.
10. Sergeeva EG, Espinosa-Garcia C, Atif F, Pardue MT, Stein DG. Neurosteroid allopregnanolone reduces ipsilateral visual cortex potentiation following unilateral optic nerve injury. *Exp Neurol*. 2018;306:138–148.
11. Sala C, Segal M. Dendritic spines: the locus of structural and functional plasticity. *Physiol Rev*. 2014;94:141–188.
12. Holtmaat A, Svoboda K. Experience-dependent structural synaptic plasticity in the mammalian brain. *Nat Rev Neurosci*. 2009;10:647–658.
13. Navarrete M, Perea G, Fernandez de Sevilla D, et al. Astrocytes mediate in vivo cholinergic-induced synaptic plasticity. *PLoS Biol*. 2012;10:e1001259.
14. Zemmar A, Chen CC, Weinmann O, et al. Oligodendrocyte- and neuron-specific Nogo-A restrict dendritic branching and spine density in the adult mouse motor cortex. *Cereb Cortex*. 2018;28:2109–2117.
15. Wu Y, Dissing-Olesen L, MacVicar BA, Stevens B. Microglia: dynamic mediators of synapse development and plasticity. *Trends Immunol*. 2015;36:605–613.
16. Monai H, Ohkura M, Tanaka M, et al. Calcium imaging reveals glial involvement in transcranial direct current stimulation-induced plasticity in mouse brain. *Nat Commun*. 2016;7:11100.
17. Liddelow SA, Guttenplan KA, Clarke LE, et al. Neurotoxic reactive astrocytes are induced by activated microglia. *Nature*. 2017;541:481–487.
18. Zhou Y, Shao A, Yao Y, Tu S, Deng Y, Zhang J. Dual roles of astrocytes in plasticity and reconstruction after traumatic brain injury. *Cell Commun Signal*. 2020;18:62.
19. Miyamoto N, Magami S, Inaba T, et al. The effects of A1/A2 astrocytes on oligodendrocyte linage cells against white matter injury under prolonged cerebral hypoperfusion. *Glia*. 2020;68:1910–1924.
20. Zamanian JL, Xu L, Foo LC, et al. Genomic analysis of reactive astrogliosis. *J Neurosci*. 2012;32:6391–6410.
21. Bergami M, Santi S, Formaggio E, et al. Uptake and recycling of pro-BDNF for transmitter-induced secretion by cortical astrocytes. *J Cell Biol*. 2008;183:213–221.
22. Park H, Poo MM. Neurotrophin regulation of neural circuit development and function. *Nat Rev Neurosci*. 2013;14:7–23.
23. Moya-Alvarado G, Gonzalez A, Stuardo N, Bronfman FC. Brain-derived neurotrophic factor (BDNF) regulates Rab5-positive early endosomes in hippocampal neurons to induce dendritic branching. *Front Cell Neurosci*. 2018;12:493.
24. Lazo OM, Gonzalez A, Ascano M, Kuruvilla R, Couve A, Bronfman FC. BDNF regulates Rab11-mediated recycling endosome dynamics to induce dendritic branching. *J Neurosci*. 2013;33:6112–6122.
25. Hyttinen JM, Niittykoski M, Salminen A, Kaarniranta K. Maturation of autophagosomes and endosomes: a key role for Rab7. *Biochim Biophys Acta*. 2013;1833:503–510.
26. Nikoletopoulou V, Sidiropoulou K, Kallergi E, Dalezios Y, Tavernarakis N. Modulation of autophagy by BDNF underlies synaptic plasticity. *Cell Metab*. 2017;26:230–242.e235.
27. Levkovitch-Verbin H, Harris-Cerruti C, Groner Y, Wheeler LA, Schwartz M, Yoles E. RGC death in mice after optic nerve crush injury: oxidative stress and neuroprotection. *Invest Ophthalmol Vis Sci*. 2000;41:4169–4174.
28. Tezel G, Yang X, Yang J, Wax MB. Role of tumor necrosis factor receptor-1 in the death of retinal ganglion cells following optic nerve crush injury in mice. *Brain Res*. 2004;996:202–212.
29. Gabriele ML, Ishikawa H, Schuman JS, et al. Optic nerve crush mice followed longitudinally with spectral domain optical coherence tomography. *Invest Ophthalmol Vis Sci*. 2011;52:2250–2254.
30. Lai CSW, Adler A, Gan WB. Fear extinction reverses dendritic spine formation induced by fear conditioning in the mouse auditory cortex. *Proc Natl Acad Sci USA*. 2018;115:9306–9311.
31. Lukasiewicz K, Robacha M, Bozycki L, Radwanska K, Czajkowski R. Simultaneous two-photon in vivo imaging of synaptic inputs and postsynaptic targets in the mouse retrosplenial cortex. *J Vis Exp*. 2016;109:53528.
32. Grutzendler J, Yang G, Pan F, Parkhurst CN, Gan WB. Transcranial two-photon imaging of the living mouse brain. *Cold Spring Harbor Protoc*. 2011;2011:21880826.
33. Quan Y, Wu Y, Zhan Z, et al. Inhibition of the leucine-rich repeat protein lingo-1 enhances RGC survival in optic nerve injury. *Exp Ther Med*. 2020;19:619–629.
34. Paxinos G, Franklin KBJ. *Paxinos and Franklin's the mouse brain in stereotaxic coordinates*. 4th ed. Amsterdam: Elsevier/AP; 2013.
35. Ylä-Anttila P, Vihinen H, Jokitalo E, Eskelinen EL. Monitoring autophagy by electron microscopy in mammalian cells. *Methods Enzymol*. 2009;452:143–164.
36. Klionsky DJ, Abdelmohsen K, Abe A, et al. Guidelines for the use and interpretation of assays for monitoring autophagy (3rd edition). *Autophagy*. 2016;12:1–222.
37. Bhatt DH, Zhang S, Gan WB. Dendritic spine dynamics. *Annu Rev Physiol*. 2009;71:261–282.
38. Montey KL, Quinlan EM. Recovery from chronic monocular deprivation following reactivation of thalamocortical plasticity by dark exposure. *Nat Commun*. 2011;2:317.
39. Grutzendler J, Kasthuri N, Gan WB. Long-term dendritic spine stability in the adult cortex. *Nature*. 2002;420:812–816.
40. Majewska AK, Newton JR, Sur M. Remodeling of synaptic structure in sensory cortical areas in vivo. *J Neurosci*. 2006;26:3021–3029.
41. Tjia M, Yu X, Jammu LS, Lu J, Zuo Y. Pyramidal neurons in different cortical layers exhibit distinct dynamics and plasticity of apical dendritic spines. *Front Neural Circuits*. 2017;11:43.
42. Mataga N, Mizuguchi Y, Hensch TK. Experience-dependent pruning of dendritic spines in visual cortex by tissue plasminogen activator. *Neuron*. 2004;44:1031–1041.
43. Sofroniew MV, Vinters HV. Astrocytes: biology and pathology. *Acta Neuropathol*. 2010;119:7–35.
44. Liddelow SA, Barres BA. Reactive astrocytes: production, function, and therapeutic potential. *Immunity*. 2017;46:957–967.
45. Raiker SJ, Lee H, Baldwin KT, Duan Y, Shrager P, Giger RJ. Oligodendrocyte-myelin glycoprotein and Nogo negatively regulate activity-dependent synaptic plasticity. *J Neurosci*. 2010;30:12432–12445.
46. Sipe GO, Lowery RL, Tremblay ME, Kelly EA, Lamantia CE, Majewska AK. Microglial P2Y12 is necessary for synaptic plasticity in mouse visual cortex. *Nat Commun*. 2016;7:10905.
47. Tremblay ME, Lowery RL, Majewska AK. Microglial interactions with synapses are modulated by visual experience. *PLoS Biol*. 2010;8:e1000527.
48. Schecter RW, Maher EE, Welsh CA, Stevens B, Erisir A, Bear MF. Experience-dependent synaptic plasticity in V1 occurs without microglial CX3CR1. *J Neurosci*. 2017;37:10541–10553.
49. Wong EL, Lutz NM, Hogan VA, et al. Developmental alcohol exposure impairs synaptic plasticity without overtly altering microglial function in mouse visual cortex. *Brain Behav Immun*. 2018;67:257–278.
50. Ahlers KE, Karaçay B, Fuller L, Bonthius DJ, Dailey ME. Transient activation of microglia following acute alcohol exposure in developing mouse neocortex is primarily driven

Investigative Ophthalmology & Visual Science

Downloaded from iovs.arvojournals.org on 01/17/2022

by BAX-dependent neurodegeneration. *Glia*, 2015;63:1694–1713.

51. Caleo M, Menna E, Chierzi S, Cenni MC, Maffei L. Brain-derived neurotrophic factor is an anterograde survival factor in the rat visual system. *Curr Biol*. 2000;10:1155–1161.
52. Spalding KL, Tan MM, Hendry IA, Harvey AR. Anterograde transport and trophic actions of BDNF and NT-4/5 in the developing rat visual system. *Mol Cell Neurosci*. 2002;19:485–500.
53. Caleo M, Medini P, von Bartheld CS, Maffei L. Provision of brain-derived neurotrophic factor via anterograde transport from the eye preserves the physiological responses of axotomized geniculate neurons. *J Neurosci*. 2003;23:287–296.
54. Dekeyster E, Geeraerts E, Buyens T, et al. Tackling glaucoma from within the brain: an unfortunate interplay of BDNF and TrkB. *PLoS One*. 2015;10:e0142067.
55. Viegi A, Cotrufo T, Berardi N, Mascia L, Maffei L. Effects of dark rearing on phosphorylation of neurotrophin Trk receptors. *Eur J Neurosci*. 2002;16:1925–1930.
56. Howe CL, Mobley WC. Signaling endosome hypothesis: a cellular mechanism for long distance communication. *J Neurobiol*. 2004;58:207–216.
57. Kononenko NL, Classen GA, Kuijpers M, et al. Retrograde transport of TrkB-containing autophagosomes via the adaptor AP-2 mediates neuronal complexity and prevents neurodegeneration. *Nat Commun*. 2017;8:14819.
58. Yoshii A, Constantine-Paton M. Postsynaptic BDNF-TrkB signaling in synapse maturation, plasticity, and disease. *Dev Neurobiol*. 2010;70:304–322.
59. Ginsberg SD, Che S, Wuu J, Counts SE, Mufson EJ. Down regulation of trk but not p75NTR gene expression in single cholinergic basal forebrain neurons mark the progression of Alzheimer's disease. *J Neurochem*. 2006;97:475–487.
60. Ginsberg SD, Mufson EJ, Counts SE, et al. Regional selectivity of rab5 and rab7 protein upregulation in mild cognitive impairment and Alzheimer's disease. *J Alzheimers Dis*. 2010;22:631–639.
61. Liu S, Li X. Regulation of autophagy in neurodegenerative diseases by natural products. *Adv Exp Med Biol*. 2020;1207:725–730.
62. Li X, Valencia A, Sapp E, et al. Aberrant Rab11-dependent trafficking of the neuronal glutamate transporter EAAC1 causes oxidative stress and cell death in Huntington's disease. *J Neurosci*. 2010;30:4552–4561.

Investigative Ophthalmology & Visual Science

Downloaded from iovs.arvojournals.org on 01/17/2022